

CoIn-SafeLink: Safety-critical Control With Cost-sensitive Incremental Random Vector Functional Link Network

Songqiao Hu¹, Zeyi Liu¹, Xiao He¹ and Zhen Shen²

Abstract—Control barrier functions (CBFs) play a crucial role in achieving the safety-critical control of robotic systems theoretically. However, most existing methods rely on the analytical expressions of unsafe state regions, which is often impractical for irregular and dynamic unsafe regions. In this paper, a novel CBF construction approach, called CoIn-SafeLink, is proposed based on cost-sensitive incremental random vector functional-link (RVFL) neural networks. By designing an appropriate cost function, CoIn-SafeLink achieves differentiated sensitivities to safe and unsafe samples, effectively achieving zero false-negative risk in unsafe sample classification. Additionally, an incremental update theorem for CoIn-SafeLink is proposed, enabling precise adjustments in response to changes in the unsafe region. Finally, the gradient analytical expression of the CoIn-SafeLink is provided to calculate the control input. The proposed method is validated on a 3-degree-of-freedom drone attitude control system. Experimental results demonstrate that the method can effectively learn the unsafe region boundaries and rapidly adapt as these regions evolve, with an update speed approximately five times faster than comparison methods. The source code is available at <https://github.com/songqiaohu/CoIn-SafeLink>.

I. INTRODUCTION

The safety of dynamic systems has long been a critical focus of research in autonomous systems, which is defined as the ability of the system to prevent harm to personnel, equipment, or the environment [1]. With the continuous advancement of modern intelligent control theory, the operational safety of intelligent agents (e.g., robots) is considered a key factor in successfully executing tasks. It is typically essential to first assess the safety of system states effectively, followed by the design of control algorithms aimed at mitigating potential risks [2]. Therefore, how to design control algorithms to ensure safe-critical control has become an increasingly important research area.

The safety of control systems can be represented by the constraints in states and can be specified in terms of the invariant set [3]. In this context, control barrier functions method has emerged as a potential control scheme recently for ensuring the safety of systems, due to its theoretical

guarantees and real-time performance [4]. CBFs extend the concept of barrier functions by incorporating the control input, allowing the system to satisfy safety conditions through appropriate adjustments [5], [6]. Given a safety set and a nominal controller without safety constraints, control strategies based on CBFs typically formulate a *quadratic programming* (QP) problem, incorporating the CBF condition as a constraint while minimizing deviation from the nominal controller. Building on this, several studies have successfully applied the CBF method in domains such as robotic manipulation [7], autonomous driving [8], and satellite trajectory control [9], yielding promising results.

A key prerequisite for the CBF method is to fully understand knowledge of unsafe regions in system states and be able to express it in explicit mathematical form. However, due to the complexity of real systems, the randomness and non-stationarity of the real world, the unsafe regions of system states are often irregular [10], making it challenging to derive analytical expressions for CBFs. In addition, although analytical expressions can be formulated in some scenarios, they may consist of numerous and complex functions, requiring significant time and effort to compute. To address these challenges, recent studies have explored the construction of CBFs using data sampling and machine learning techniques. In these studies, datasets consisting of system states and safety levels are typically collected via sensors or provided in a human-in-the-loop mode. A classifier is then employed to learn the CBFs. In this paradigm, several support vector machine (SVM)-based methods [11], [12] and multilayer perceptron (MLP)-based methods [13], [14] have been developed for constructing CBFs.

However, the aforementioned machine learning-based methods still have some limitations that require further attention. In most scenarios, the safety constraints and the extent of human understanding of safety threats are constantly evolving [15], [16]. This characteristic imposes certain requirements on the incremental update capability of CBFs, particularly with regard to speed and real-time performance. Moreover, these machine learning methods often fail to provide gradient expressions, which limits their applicability when further exploring the properties of the constructed CBFs.

To address the aforementioned issues, we propose a new real-time safety-critical control strategy CoIn-SafeLink that constructs more effective CBFs to cope with changing safety threats. The main contributions of this work are as follows:

- 1) The CBF is constructed using a cost-sensitive incremental random vector functional link network strategy,

*This work was supported by National Natural Science Foundation of China under grants 62473223, 624B2087 and Beijing Natural Science Foundation under grant L241016. (Corresponding author: Xiao He)

¹ Songqiao Hu, Zeyi Liu, and Xiao He are with the Department of Automation, Tsinghua University, Beijing 100084, China (e-mails: hsq23@mails.tsinghua.edu.cn; liuzy21@mails.tsinghua.edu.cn; hexiao@tsinghua.edu.cn).

² Zhen Shen is with State Key Laboratory of Multimodal Artificial Intelligence Systems, Beijing Engineering Research Center of Intelligent Systems and Technology, Institute of Automation, Chinese Academy of Sciences (e-mail: zhen.shen@ia.ac.cn).

trained on a dataset containing both safe and unsafe samples. A novel objective function is designed to incorporate cost sensitivity, ensuring that the unsafe region is included within the boundary of designed CBF.

- 2) A precise incremental update theorem and corresponding gradient expressions are derived, enabling the designed CBF to adapt in real time to changing safety constraints.
- 3) The proposed method is validated on a second-order drone attitude control system, demonstrating its practical effectiveness.

The remainder of the paper is organized as follows: Section II provides the preliminaries on CBFs and RVFL. Section III describes the proposed safety-critical control strategy, while Section IV presents the experimental results on a drone attitude control system. Finally, the paper concludes in Section V.

II. PRELIMINARIES

A. Control Barrier Function

Consider the following affine control system:

$$\dot{\mathbf{x}} = \mathbf{f}(\mathbf{x}) + \mathbf{g}(\mathbf{x})\mathbf{u}, \quad (1)$$

where $\mathbf{x} \in \mathbb{R}^n$, $\mathbf{f} : \mathbb{R}^n \rightarrow \mathbb{R}^n$ and $\mathbf{g} : \mathbb{R}^n \rightarrow \mathbb{R}^{n \times q}$ is locally Lipschitz, and $\mathbf{u} \in U \subseteq \mathbb{R}^q$, where U is the control constraint set defined as

$$U := \{\mathbf{u} \in \mathbb{R}^q : -\mathbf{u}_{\min} \leq \mathbf{u} \leq \mathbf{u}_{\max}\}, \quad (2)$$

with $\mathbf{u}_{\min}, \mathbf{u}_{\max} \in \mathbb{R}^q$ and the inequalities are interpreted element-wise.

Definition 1: (Class \mathcal{K} function [17]) A continuous function $\alpha : [0, a) \rightarrow [0, \infty)$, $a > 0$, is said to belong to class \mathcal{K} if it is strictly increasing and $\alpha(0) = 0$.

Definition 2: (Relative Degree) The relative degree of a differentiable function $B : \mathbb{R}^n \rightarrow \mathbb{R}$ with respect to system (1) is the number of times it needs to be differentiated along its dynamics until the control \mathbf{u} explicitly shows in the corresponding derivative.

Definition 3: A set $C \subset \mathbb{R}^n$ is forward invariant for system (1) if its solutions starting at any $\mathbf{x}(t_0) \in C$ satisfy $\mathbf{x}(t) \in C$, $\forall t \geq t_0$.

Let

$$C := \{\mathbf{x} \in \mathbb{R}^n : B(\mathbf{x}) \geq 0\}, \quad (3)$$

where $B : \mathbb{R}^n \rightarrow \mathbb{R}$ is a continuously differentiable function.

Definition 4: (Control barrier function [18]) Given a set C as in Eq. (3), $B(\mathbf{x})$ is a control barrier function (CBF) for system (1) if there exists a class \mathcal{K} function α such that

$$\sup_{\mathbf{u} \in U} [L_f B(\mathbf{x}) + L_g B(\mathbf{x})\mathbf{u} + \alpha(B(\mathbf{x}))] \geq 0, \quad \forall \mathbf{x} \in C, \quad (4)$$

where L_f, L_g denote the Lie derivatives along f and g , respectively.

Lemma 1: [19] Given a CBF $B(\mathbf{x})$ from Def. 4 with the associated set C defined by Eq. (3), if $\mathbf{x}(t_0) \in C$, then any Lipschitz continuous controller $\mathbf{u}(t)$ that satisfies the

constraint in Eq. (4), $\forall t \geq t_0$ renders C forward invariant for system (1).

B. High-order Control Barrier Function

For a control barrier function $B(\mathbf{x})$ with relative degree r , define $\psi_0(\mathbf{x}) := B(\mathbf{x})$ and a sequence of functions $\psi_i : \mathbb{R}^n \rightarrow \mathbb{R}, i \in \{1, \dots, r-1\}$:

$$\psi_i(\mathbf{x}) := \dot{\psi}_{i-1}(\mathbf{x}) + \alpha_i(\psi_{i-1}(\mathbf{x})), i \in \{1, \dots, r-1\}, \quad (5)$$

where $\alpha_i(\cdot)$ denotes a class \mathcal{K} function. Define a sequence of sets $C_i, i \in \{1, \dots, r\}$ associated with Eq. (5) in the form:

$$C_i := \{\mathbf{x} \in \mathbb{R}^n : \psi_{i-1}(\mathbf{x}) \geq 0\}, i \in \{1, \dots, r\}. \quad (6)$$

Definition 5: (High Order Control Barrier Function [20]) Let C_1, C_2, \dots, C_r be defined by Eq. (6) and $\psi_1(\mathbf{x}), \dots, \psi_{r-1}(\mathbf{x})$ be defined by Eq. (5). A function $B : \mathbb{R}^n \rightarrow \mathbb{R}$ is a High order control barrier function (HOCBF) of relative degree r for system (1) if there exist differentiable class \mathcal{K} functions $\alpha_i, i \in \{1, \dots, r-1\}$ and a class \mathcal{K} function α_r such that

$$\sup_{\mathbf{u} \in U} [L_f^r B(\mathbf{x}) + L_g L_f^{r-1} B(\mathbf{x})\mathbf{u} + \mathcal{O}(B(\mathbf{x})) + \alpha_r(\psi_{r-1}(\mathbf{x}))] \geq 0, \quad \forall \mathbf{x} \in C_1 \cap C_2 \cap \dots \cap C_r, \quad (7)$$

where L_f^r denotes Lie derivatives along f r times, $\mathcal{O}(B(\mathbf{x})) = \sum_{i=1}^{r-1} L_f^i (\alpha_{r-i} \circ \psi_{r-i-1})(\mathbf{x})$, and $B(\mathbf{x})$ is such that $L_g L_f^{r-1} B(\mathbf{x}) \neq 0$ on the boundary of the set $C_1 \cap C_2 \cap \dots \cap C_r$.

Lemma 2: [20] Given a HOCBF $B(\mathbf{x})$ from Def. 5 with the associated sets C_1, C_2, \dots, C_r defined by Eq. (6), if $\mathbf{x}(t_0) \in C_1 \cap C_2 \cap \dots \cap C_r$, then any Lipschitz continuous controller $\mathbf{u}(t)$ that satisfies the constraint in Eq. (7), $\forall t \geq t_0$ renders $C_1 \cap C_2 \cap \dots \cap C_r$ forward invariant for system (1).

Let \mathbf{u}_r denote the reference control input, which can be determined using either optimal control or control Lyapunov functions. The control input that guarantees system safety can then be derived by

$$\mathbf{u}^* = \underset{\mathbf{u} \in U}{\operatorname{argmin}} \|\mathbf{u} - \mathbf{u}_r\|^2 \quad \text{s.t.} \quad \begin{cases} L_f B(\mathbf{x}) + L_g B(\mathbf{x})\mathbf{u} + \alpha(B(\mathbf{x})) \geq 0, \text{ if } r = 1, \\ L_f^r B(\mathbf{x}) + L_g L_f^{r-1} B(\mathbf{x})\mathbf{u} + \mathcal{O}(B(\mathbf{x})) + \alpha_r(\psi_{r-1}(\mathbf{x})) \geq 0, \text{ if } r > 1. \end{cases} \quad (8)$$

C. Random Vector Functional Link Network

RVFL is a shallow neural network architecture consisting of an input layer, an output layer, and a hidden layer [21], as illustrated in Fig. 1. The hidden layer contains N_1 node groups, each with N_2 nodes. The bias of each node within the same group is identical. Unlike traditional neural networks that are trained using gradient descent method, the training of RVFL is performed through ridge regression, which has a closed-form solution [22]. Suppose we have a lot of state samples $\{\mathbf{x}_i, \mathbf{y}_i\}, \mathbf{y}_i \in \{-1, +1\}, i \in \{1, 2, \dots, N\}$. Let $\tilde{\mathbf{x}} \in \mathbb{R}^{(m+(N_1 N_2)) \times 1}$ represent a combination of \mathbf{x} and its

enhancement features Z , and let \tilde{y} represents the one-hot coding of y :

$$\tilde{x} = \begin{bmatrix} \mathbf{x}^\top \\ \mathbf{Z}^\top \end{bmatrix} = \begin{bmatrix} \mathbf{x}^\top \\ \phi(\mathbf{x}^\top \mathbf{W}_{e_1} + \mathbf{b}_{e_1}) \\ \phi(\mathbf{x}^\top \mathbf{W}_{e_2} + \mathbf{b}_{e_2}) \\ \vdots \\ \phi(\mathbf{x}^\top \mathbf{W}_{e_{N_1}} + \mathbf{b}_{e_{N_1}}) \end{bmatrix},$$

$$\tilde{y} = \begin{cases} [1, 0], & \text{if } y = -1 \\ [0, 1], & \text{if } y = +1, \end{cases} \quad (9)$$

where $\phi(\cdot) : \mathbb{R} \rightarrow \mathbb{R}$ is an activation function, both $\mathbf{W}_e = [\mathbf{W}_{e_1}, \mathbf{W}_{e_2}, \dots, \mathbf{W}_{e_{N_1}}]$ and $\mathbf{b}_e = [\mathbf{b}_{e_1}, \mathbf{b}_{e_2}, \dots, \mathbf{b}_{e_{N_1}}]$ are randomly initialized. If the input of $\phi(\cdot)$ is a matrix, the function $\phi(\cdot)$ is applied element-wise to the matrix.

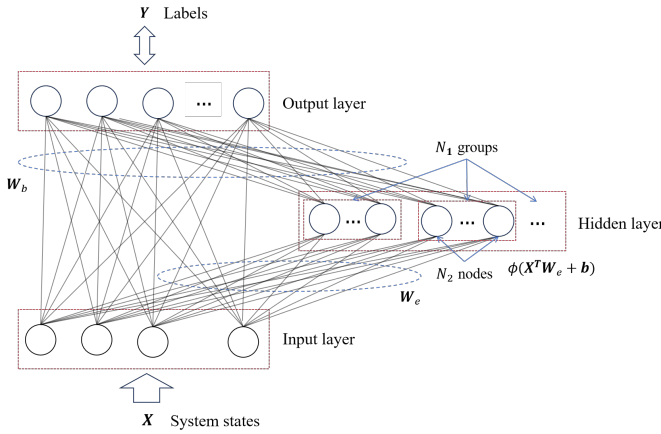


Fig. 1. Architecture of RVFL. \mathbf{W}_e represents the randomly initialized and fixed weights, while \mathbf{W}_b denotes the weights obtained through ridge regression.

Denote the extended data matrix and label matrix as

$$\mathbf{A} = [\tilde{\mathbf{x}}_1^\top, \tilde{\mathbf{x}}_2^\top, \dots, \tilde{\mathbf{x}}_N^\top]^\top, \mathbf{Y} = [\tilde{\mathbf{y}}_1^\top, \tilde{\mathbf{y}}_2^\top, \dots, \tilde{\mathbf{y}}_N^\top]^\top, \quad (10)$$

where the training of RVFL is summarized as solving the optimization problem in Eq. (11) to obtain \mathbf{W}_b :

$$\mathbf{W}_b = \arg \min_{\mathbf{W}} \lambda \|\mathbf{W}\|_2^2 + \|\mathbf{A}\mathbf{W} - \mathbf{Y}\|_2^2, \quad (11)$$

$$\mathbf{W}_b = (\lambda \mathbf{I} + \mathbf{A}^\top \mathbf{A})^{-1} \mathbf{A}^\top \mathbf{Y}. \quad (12)$$

Lemma 3: (Woodbury Formula [23]) $\mathbf{A}, \mathbf{U}, \mathbf{C}$ and \mathbf{V} are conformable matrices: $\mathbf{A} \in \mathbb{R}^{n \times n}$, $\mathbf{C} \in \mathbb{R}^{k \times k}$, $\mathbf{U} \in \mathbb{R}^{n \times k}$, and $\mathbf{V} \in \mathbb{R}^{k \times n}$. The Woodbury formula is

$$(\mathbf{A} + \mathbf{UCV})^{-1} = \mathbf{A}^{-1} - \mathbf{A}^{-1} \mathbf{U} (\mathbf{C}^{-1} + \mathbf{V} \mathbf{A}^{-1} \mathbf{U})^{-1} \mathbf{V} \mathbf{A}^{-1}. \quad (13)$$

III. THE PROPOSED SAFETY-CRITICAL CONTROL STRATEGY

A. Coln-SafeLink Design and Control for Systems

We propose the cost-sensitive incremental RVFL by modifying the cost function in Eq. (11), making it more suitable for safety-critical control scenarios.

Let the cost of misclassifying a sample of -1 as $+1$ is c_1 , and the cost of misclassifying a sample of $+1$ as -1 is c_2 . The cost matrix \mathbf{C} is defined as:

$$\mathbf{C} = \begin{bmatrix} 0 & c_1 \\ c_2 & 0 \end{bmatrix}. \quad (14)$$

Based on the idea of cross-entropy, the dot product of $\mathbf{A}\mathbf{W}$ and \mathbf{Y} reflects the degree of deviation between $\mathbf{A}\mathbf{W}$ and \mathbf{Y} . Therefore, the cost-sensitive term designed is $tr(\mathbf{A}\mathbf{W}\mathbf{C}^\top \mathbf{Y}^\top)$, where tr denotes the trace of a matrix. New cost function is shown in Eq. (15):

$$\mathbf{W}_b = \arg \min_{\mathbf{W}} \lambda_1 \|\mathbf{W}\|_2^2 + \lambda_2 \|\mathbf{A}\mathbf{W} - \mathbf{Y}\|_2^2 + \underbrace{2tr(\mathbf{A}\mathbf{W}\mathbf{C}^\top \mathbf{Y}^\top)}_{\text{Cost-sensitive term}}. \quad (15)$$

It is worth mentioning that the cost-sensitive term is not written as a summation of sample-level costs, as in SVM [11] or MLP [13], because this form does not allow for differentiation with respect to the weight matrix \mathbf{W}_b , thus losing the ability for incremental updates. In contrast, $tr(\mathbf{A}\mathbf{W}\mathbf{C}^\top \mathbf{Y}^\top)$ can be differentiated with respect to \mathbf{W}_b , which is crucial for the derivation of the incremental update expression.

From convex optimization theory, the \mathbf{W}_b corresponding to Eq. (15) should satisfy

$$2\lambda_1 \mathbf{W}_b + 2\lambda_2 \mathbf{A}^\top (\mathbf{A}\mathbf{W}_b - \mathbf{Y}) + 2\mathbf{A}^\top \mathbf{Y} \mathbf{C} = \mathbf{0}, \quad (16)$$

which leads to

$$\mathbf{W}_b = \underbrace{(\lambda_1 \mathbf{I} + \lambda_2 \mathbf{A}^\top \mathbf{A})^{-1}}_{\mathbf{K}} \underbrace{(\lambda_2 \mathbf{A}^\top \mathbf{Y} - \mathbf{A}^\top \mathbf{Y} \mathbf{C})}_{\mathbf{Q}}. \quad (17)$$

For a state sample \mathbf{x} , with reference to Eqs. (9)(10)(17), its prediction confidence $\hat{\mathbf{Y}} \in \mathbb{R}^{1 \times 2}$ is

$$\begin{aligned} \hat{\mathbf{Y}} &= \tilde{\mathbf{x}}^\top \mathbf{W}_b \\ &= \tilde{\mathbf{x}}^\top (\lambda_1 \mathbf{I} + \lambda_2 \mathbf{A}^\top \mathbf{A})^{-1} (\lambda_2 \mathbf{A}^\top \mathbf{Y} - \mathbf{A}^\top \mathbf{Y} \mathbf{C}) \\ &= \mathbf{x}^\top \mathbf{W}_{b_0} + \sum_{i=1}^{N_1} \sum_{j=1}^{N_2} \phi(\mathbf{x}^\top \mathbf{W}_{e_{i,j}} + b_{e_{i,j}}) \mathbf{W}_{b_{i,j}}, \end{aligned} \quad (18)$$

where $\mathbf{W}_{b_0} \in \mathbb{R}^{m \times 2}$ represents the submatrix of \mathbf{W}_b corresponding to \mathbf{x}^\top , $\mathbf{W}_{b_{i,j}} \in \mathbb{R}^{1 \times 2}$ represents the submatrix of \mathbf{W}_b corresponding to the j -th feature node of the i -th feature group, the same as $b_{e_{i,j}} \in \mathbb{R}$, and $\mathbf{W}_{e_{i,j}} \in \mathbb{R}^m$ represents the weight matrix corresponding to the j -th node of the i -th group.

Since $\hat{\mathbf{Y}}$ is a vector but the value of the CBF should be a scalar, a conversion is required. Considering that if $\hat{\mathbf{Y}} = [0, 1]$, CBF is expected to output $+1$; if $\hat{\mathbf{Y}} = [1, 0]$, is expected to output -1 ; and if $\hat{\mathbf{Y}} = [0.5, 0.5]$, is expected to output 0 . Thus, the CBF is constructed as Eq. (19), which remains continuously differentiable with respect to \mathbf{x} :

$$B(\mathbf{x}) = 2\hat{\mathbf{Y}} [0, 1]^\top - 1. \quad (19)$$

Eqs. (18)(19) indicate that solving for the control input requires knowledge of the gradient of the CBF. Taking the

first-order and second-order gradient of Eq. (19), we have:

$$\begin{aligned}\nabla_{\mathbf{x}}B &= 2\mathbf{W}_{b_0} [0, 1]^\top + \\ & 2 \sum_{i=1}^{N_1} \sum_{j=1}^{N_2} \mathbf{W}_{b_{i,j}} \begin{bmatrix} 0 \\ 1 \end{bmatrix} \phi'(\mathbf{x}^\top \mathbf{W}_{e_{i,j}} + b_{e_{i,j}}) \mathbf{W}_{e_{i,j}}, \\ \nabla_{\mathbf{x}}^2 B &= \frac{\partial^2 B}{\partial \mathbf{x} \partial \mathbf{x}^\top} \\ &= 2 \sum_{i=1}^{N_1} \sum_{j=1}^{N_2} \mathbf{W}_{b_{i,j}} \begin{bmatrix} 0 \\ 1 \end{bmatrix} \phi''(\mathbf{x}^\top \mathbf{W}_{e_{i,j}} + B_{e_{i,j}}) \mathbf{W}_{e_{i,j}} \mathbf{W}_{e_{i,j}}^\top.\end{aligned}\quad (20)$$

If the CBF has a relative degree of 1 with respect to the system, then $L_f B = \nabla_{\mathbf{x}} B \cdot f(\mathbf{x})$ and $L_g B = \nabla_{\mathbf{x}} B \cdot g(\mathbf{x})$ can be substituted into Eq. (8) to solve for \mathbf{u}^* . For systems with a relative degree of 2, the following Lie derivatives need to be computed:

$$\nabla_{\mathbf{x}}(L_f B) = \nabla_{\mathbf{x}}^2 B^\top \cdot \mathbf{f} + \left(\frac{\partial \mathbf{f}}{\partial \mathbf{x}^\top} \right)^\top \cdot \nabla_{\mathbf{x}} B,$$

$$L_f^2 B = \nabla_{\mathbf{x}}(L_f B) \cdot \mathbf{f}, \quad L_g L_f B = \nabla_{\mathbf{x}}(L_f B) \cdot \mathbf{g}. \quad (21)$$

For higher-order systems, the calculation of the Lie derivatives follows a similar approach. It is important to note that for a system with a relative order r , the activation function must be selected to be r -times differentiable. The control input is then determined to achieve safety-critical control by solving the QP in Eq. (8).

B. Update of CoIn-SafeLink

When the unsafe region changes, CoIn-SafeLink can perform incremental updates using the newly collected samples, eliminating the need to retrain on the entire dataset.

Theorem 1: Denote the original extended matrix of the available samples at time t as \mathbf{A}_t , the safety level matrix as \mathbf{Y}_t , and the CBF as $B_t(\mathbf{x})$. If ΔN new samples are collected at time $t+1$, assuming the new extended data matrix is $\Delta \mathbf{A}$ and the new level matrix is $\Delta \mathbf{Y}$, then

$$B_{t+1}(\mathbf{x}) = B_t(\mathbf{x}) + 2\tilde{\mathbf{x}}^\top (\mathbf{K}_t \Delta \mathbf{Q} - \Delta \mathbf{K} \mathbf{Q}_t - \Delta \mathbf{K} \Delta \mathbf{Q}) \begin{bmatrix} 0 \\ 1 \end{bmatrix}, \quad (22)$$

where

$$\mathbf{K}_t = (\lambda_1 \mathbf{I} + \lambda_2 \mathbf{A}_t^\top \mathbf{A}_t)^{-1},$$

$$\mathbf{Q}_t = \lambda_2 \mathbf{A}_t^\top \mathbf{Y}_t - \mathbf{A}_t^\top \mathbf{Y}_t \mathbf{C},$$

$$\Delta \mathbf{K} = \lambda_2 \mathbf{K}_t \Delta \mathbf{A}^\top (\mathbf{I} + \lambda_2 \Delta \mathbf{A} \mathbf{K}_t \Delta \mathbf{A}^\top)^{-1} \Delta \mathbf{A} \mathbf{K}_t,$$

$$\Delta \mathbf{Q} = \Delta \mathbf{A}^\top \Delta \mathbf{Y} - \Delta \mathbf{A}^\top \Delta \mathbf{Y} \mathbf{C}.$$

Proof Let the extended matrix of available samples at time $t+1$ be given by:

$$\mathbf{A}_{t+1} = \begin{bmatrix} \mathbf{A}_t \\ \Delta \mathbf{A} \end{bmatrix}, \quad \mathbf{Y}_{t+1} = \begin{bmatrix} \mathbf{Y}_t \\ \Delta \mathbf{Y} \end{bmatrix}. \quad (23)$$

According to Eqs. (12)(23), the weight matrix \mathbf{W}_b at time $t+1$ can be expressed as:

$$\begin{aligned}\mathbf{W}_{b,t+1} &= \underbrace{(\lambda_1 \mathbf{I} + \lambda_2 \mathbf{A}_t^\top \mathbf{A}_t + \lambda_2 \Delta \mathbf{A}^\top \Delta \mathbf{A})^{-1}}_{\mathbf{K}_{t+1}} \cdot \\ & \underbrace{(\lambda_2 \mathbf{A}_t^\top \mathbf{Y}_t + \lambda_2 \Delta \mathbf{A}^\top \Delta \mathbf{Y} - \mathbf{A}_t^\top \mathbf{Y}_t \mathbf{C} - \Delta \mathbf{A}^\top \Delta \mathbf{Y} \mathbf{C})}_{\mathbf{Q}_{t+1}}.\end{aligned}\quad (24)$$

Based on Lemma 3, \mathbf{K}_{t+1} and \mathbf{Q}_{t+1} in Eq. (24) can be transformed into:

$$\mathbf{K}_{t+1} = \mathbf{K}_t - \underbrace{\lambda_2 \mathbf{K}_t \Delta \mathbf{A}^\top (\mathbf{I} + \lambda_2 \Delta \mathbf{A} \mathbf{K}_t \Delta \mathbf{A}^\top)^{-1} \Delta \mathbf{A} \mathbf{K}_t}_{\Delta \mathbf{K}}, \quad (25)$$

and

$$\mathbf{Q}_{t+1} = \mathbf{Q}_t + \underbrace{\lambda_2 \Delta \mathbf{A}^\top \Delta \mathbf{Y} - \Delta \mathbf{A}^\top \Delta \mathbf{Y} \mathbf{C}}_{\Delta \mathbf{Q}}. \quad (26)$$

Combining Eqs. (12) and (24)-(26), we obtain

$$\begin{aligned}\mathbf{W}_{b,t+1}(\mathbf{x}) &= (\mathbf{K}_t - \Delta \mathbf{K})(\mathbf{Q}_t + \Delta \mathbf{Q}) \\ &= \mathbf{W}_{b,t} + \mathbf{K}_t \Delta \mathbf{Q} - \Delta \mathbf{K} \mathbf{Q}_t - \Delta \mathbf{K} \Delta \mathbf{Q},\end{aligned}\quad (27)$$

which leads to

$$\begin{aligned}B_{t+1}(\mathbf{x}) &= 2\tilde{\mathbf{x}}^\top \mathbf{W}_{b,t+1} [0, 1]^\top - 1 \\ &= B_t(\mathbf{x}) + 2\tilde{\mathbf{x}}^\top (\mathbf{K}_t \Delta \mathbf{Q} - \Delta \mathbf{K} \mathbf{Q}_t - \Delta \mathbf{K} \Delta \mathbf{Q}) [0, 1]^\top.\end{aligned}\quad (28)$$

□

Remark 1: Since the number of rows and columns of $\lambda_2 \Delta \mathbf{A} \mathbf{K}_t \Delta \mathbf{A}^\top$ (a square matrix) is equal to the number of new samples ΔN , the time complexity of computing the inverse matrix in $\Delta \mathbf{K}$ is approximately $\mathcal{O}(\Delta N^3)$. Typically, the number of newly collected samples is much smaller than the total number of samples used in the offline training stage. Therefore, the computational cost of incrementally updating the CBF is significantly lower than that of retraining the CBF using the entire dataset.

The procedure of Coin-SafeLink is formalized in Algorithm 1, which operates in three stages. In the offline stage, the CBF $B_t(\mathbf{x})$ is constructed using the training dataset, as outlined in lines 1-4. During the control stage, the reference control input \mathbf{u}_r and the Lie derivative of $B_t(\mathbf{x})$ are utilized to derive the control input \mathbf{u}^* and update the system, as shown in lines 7-10. If the unsafe region changes, new samples are collected, and $B_t(\mathbf{x})$ is updated according to Theorem 1.

IV. EXPERIMENTS

A. Settings

We consider a second-order, 3-degree-of-freedom drone attitude control system, referred to as 3 DOF Hover. The system frame is mounted on a three degrees of freedom pivot joint that allows the body to rotate about the roll, pitch, and yaw axes [24]. The propellers are driven by four DC motors mounted at the vertices of the frame. A schematic of the

Algorithm 1: Control with learned CBF

Input: System dynamics $\dot{\mathbf{x}} = \mathbf{f}(\mathbf{x}) + \mathbf{g}(\mathbf{x})\mathbf{u}$, offline samples $\{\{\mathbf{x}_i, \mathbf{y}_i\}, 1 \leq i \leq N\}$, cost matrix \mathbf{C} , regularization parameters λ_1, λ_2 , initial state \mathbf{x}_0 , target state \mathbf{x}_e , allowed error ϵ

- 1 Initialize \mathbf{W}_e and \mathbf{b}_e in Eq. (9) randomly
- 2 Calculate \mathbf{A} and \mathbf{Y} based on Eq. (10)
- 3 Derive \mathbf{K} , \mathbf{Q} and \mathbf{W}_b according to Eq. (17)
- 4 Construct CBF $B_t(\mathbf{x})$ as shown in Eq. (19)
- 5 Set current state $\mathbf{x}_t \leftarrow \mathbf{x}_0$
- 6 **while** $\|\mathbf{x}_e - \mathbf{x}_t\|_2 > \epsilon$ **do**
- 7 Determine reference control input \mathbf{u}_r using optimal control theory
- 8 Calculate $L_f^r B, L_g L_f^{r-1} B$ similar to Eqs. (20) and (21)
- 9 Obtain \mathbf{u}^* by solving Eq. (8)
- 10 Update \mathbf{x}_t through $\dot{\mathbf{x}} = \mathbf{f}(\mathbf{x}) + \mathbf{g}(\mathbf{x})\mathbf{u}^*$
- 11 **if** *Unsafe region has changed* **then**
- 12 Collect new data samples
- 13 Calculate $\Delta\mathbf{A}$ and $\Delta\mathbf{Y}$ based on Eqs. (9)(10)
- 14 Update $B_t(\mathbf{x}), \mathbf{K}, \mathbf{Q}$ and \mathbf{W}_b according to Theorem 1
- 15 **end**
- 16 **end**

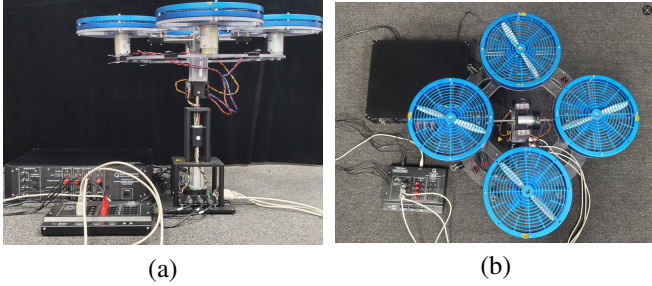


Fig. 2. Experimental 3 DOF hover platform.: (a) Front view, (b) Top view.

3 DOF Hover is shown in Fig. 2. The system states and dynamics are defined as follows:

$$\mathbf{x} = [\theta_y \quad \theta_p \quad \theta_r \quad \dot{\theta}_y \quad \dot{\theta}_p \quad \dot{\theta}_r]^\top,$$

$$\mathbf{f}(\mathbf{x}) = \begin{bmatrix} 0 & 0 & 0 & 1 & 0 & 0 \\ 0 & 0 & 0 & 0 & 1 & 0 \\ 0 & 0 & 0 & 0 & 0 & 1 \\ 0 & 0 & 0 & 0 & 0 & 0 \\ 0 & 0 & 0 & 0 & 0 & 0 \\ 0 & 0 & 0 & 0 & 0 & 0 \end{bmatrix} \mathbf{x},$$

$$\mathbf{g}(\mathbf{x}) = \begin{bmatrix} 0 & 0 & 0 & 0 \\ 0 & 0 & 0 & 0 \\ 0 & 0 & 0 & 0 \\ -\frac{K_t}{J_y} & -\frac{K_t}{J_y} & \frac{K_t}{J_y} & \frac{K_t}{J_y} \\ \frac{LK_f}{J_p} & -\frac{LK_f}{J_p} & 0 & 0 \\ 0 & 0 & \frac{LK_f}{J_r} & -\frac{LK_f}{J_r} \end{bmatrix},$$

$$\mathbf{u} = [V_f \quad V_b \quad V_r \quad V_l]^\top, \quad (29)$$

where $\theta_p, \theta_r,$ and θ_y represent the yaw, roll, and pitch, respectively, $\dot{\theta}_p, \dot{\theta}_r,$ and $\dot{\theta}_y$ represent the angular velocities, $V_f, V_b, V_r,$ and V_l represent the motor voltages, K_t and K_f represent the force constants, $J_y, J_p,$ and J_r represent the moments of inertia, and L is the distance between the propeller motor and the pivot axis. Parameters of the system are listed in Table I.

We set the activation function of the RVFL to be a variant of the Sigmoid function, specifically $f(x) = \text{sigmoid}(5x)$, with other parameters shown in Table I. The function α_2 in Eq. (7) and the function α_1 in Eq. (5) are chosen as linear functions, with linear coefficients p_2 and p_1 , respectively. For practical implementation of the control, the prediction interval is set to Δt . All these parameter values are also summarized in Table I.

TABLE I
KEY PARAMETER SPECIFICATIONS.

Parameters	K_t	K_f	J_y	J_p	J_r
Values	0.0036	0.1188	0.1104	0.0552	0.0552
Units	N·m/V	N/V	kg·m ²	kg·m ²	kg·m ²
Parameters	L	N_1	N_2	c_1	c_2
Values	0.1969	10	10	2	1
Units	m	pcs	pcs	unitless	unitless
Parameters	λ_1	λ_2	p_1	p_2	Δt
Values	0.001	5	1	1	0.05
Units	unitless	unitless	unitless	unitless	s

To highlight the necessity of the learning-based CBF construction method, we choose the irregular unsafe region that is challenging for analytically-based CBFs to be constructed. Since roll and pitch are symmetrical, we simplify the problem for clarity by assuming that the unsafe region depends only on yaw and roll. The unsafe region is formed by the union of multiple circles stacked, as shown in Fig. 3. In the offline stage, we uniformly sample 10,000 samples within the range of yaw and roll $[-1.5 \text{ rad}, 1.5 \text{ rad}]$ and assess their safety. Samples within the safe region are labeled as -1 , while those outside are labeled as $+1$.

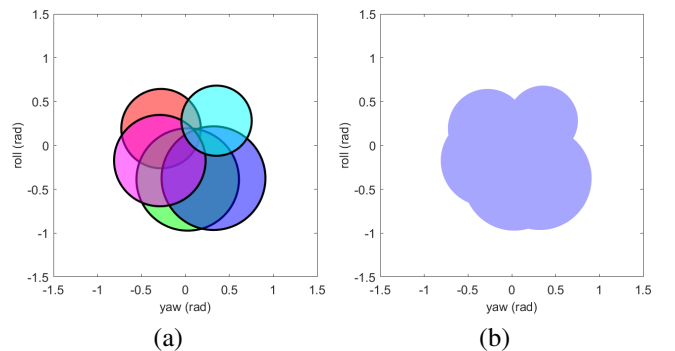


Fig. 3. Unsafe region and its generation process: (a) Use the union of overlapping circles as the unsafe region, (b) Unsafe region.

Experiments are implemented in MATLAB on a platform equipped with an Intel i5-13600KF CPU, boasting 14 cores, a 3.50-GHz clock speed, and 20 processors, complemented by 32 GB of RAM.

B. Boundary and Gradients

In this section, the boundary of the designed CBF for different values of c_1 is analyzed and the gradient of the CBF is presented to demonstrate the effectiveness of the proposed method. Table II illustrates the relationship of the boundary and samples for various values of c_1 .

As shown, $N_{u \rightarrow s}$ gradually decreases to 0 as c_1 increases, demonstrating the effectiveness of the proposed method. The CBF boundary is expected to enclose all unsafe areas, ensuring that state will never enter the unsafe region as long as it remains outside this boundary. At the same time, we aim to leave a margin to prevent the unsafe region from expanding. Therefore, $c_1 = 2.0$ is applied. Fig. 4 shows the boundary of designed $B(x)$ along with its gradients.

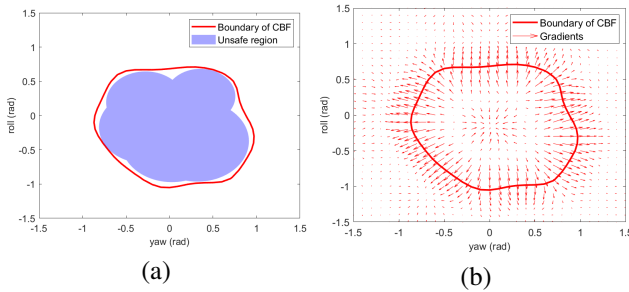


Fig. 4. Boundary and gradients: (a) Unsafe region and boundary for $c_1 = 2.0$, (b) Boundary and gradients.

As illustrated in Fig. 4(a), the boundary successfully encloses the unsafe region. Since the labels of the training samples are either -1 or $+1$, the gradients are small inside both the safe and unsafe regions, while larger near the boundary, as depicted in Fig. 4(b). Furthermore, the gradients point from the unsafe region towards the safe region, effectively preventing system states from entering the unsafe region.

C. Control and Update

The Linear Quadratic Regulator (LQR) is used to generate reference control inputs, with the cost function set as

$$J = \int_0^{\infty} (\mathbf{x}^T \mathbf{Q} \mathbf{x} + \mathbf{u}^T \mathbf{R} \mathbf{u}) dt, \quad (30)$$

where $\mathbf{Q} = \text{diag}\{500, 350, 350, 0, 20, 20\}$ is the weight of state errors and $\mathbf{R} = \text{diag}\{0.01, 0.01, 0.01, 0.01\}$ is the weight of control inputs.

The control objective is to drive the system from the initial state $\mathbf{x}_0 = [-1 \text{ rad}, 0, -1 \text{ rad}, 0, 0, 0]^T$ to target state $\mathbf{x}_f = [1.5 \text{ rad}, 0, 0, 0, 0, 0]^T$, while avoiding unsafe regions throughout the process. The unsafe region will change twice: once at $t = 3.6s$, when a circular region with a center at $\theta_y = -0.1 \text{ rad}$ and $\theta_r = -1 \text{ rad}$, with a radius of 0.15 rad, becomes unsafe; and again at $t = 8s$, when the circular region with a center at $\theta_y = 0.7 \text{ rad}$ and $\theta_r = -0.8 \text{ rad}$, with a radius of 0.15 rad, becomes unsafe. The updated

unsafe regions are shown in Fig. 5. Each time the unsafe region changes, 50 samples within the changed region will be collected to update the designed CBF.

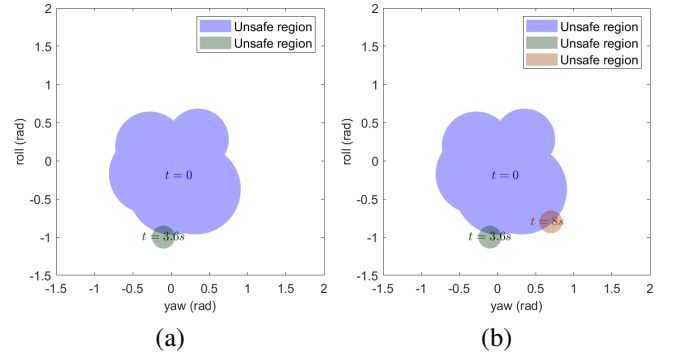


Fig. 5. Expansion of the unsafe region: (a) A circle with center at $\theta_y = -0.1 \text{ rad}$, $\theta_r = -1 \text{ rad}$, and $\text{radius} = 0.15 \text{ rad}$ at $t = 3.6s$, (b) A circle with center at $\theta_y = 0.7 \text{ rad}$, $\theta_r = -0.8 \text{ rad}$, and $\text{radius} = 0.15 \text{ rad}$ at $t = 8s$.

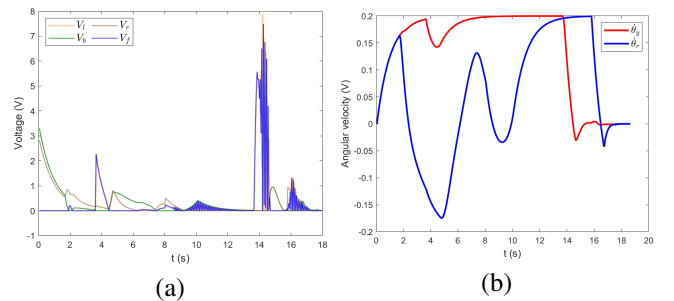


Fig. 6. Plot of (a) Voltages, (b) angular velocities.

Additionally, the input voltage range for each motor is set to $[0, 8 \text{ V}]$. To further ensure safety, $\dot{\theta}_y$ and $\dot{\theta}_r$ are restricted to $[-0.2 \text{ rad/s}, 0.2 \text{ rad/s}]$, which can also be achieved through CBFs. The voltage constraint can be directly written in inequality form as:

$$\begin{bmatrix} \text{eye}(4) \\ -\text{eye}(4) \end{bmatrix} \mathbf{u} \leq [8, 8, 8, 8, 0, 0, 0, 0]^T, \quad (31)$$

where $\text{eye}(4)$ represents a 4×4 identity matrix.

To enforce the constraint $\dot{\theta}_y \leq 0.2$, the CBF $B_{\theta}(x) = 0.2 - \dot{\theta}_y$ is constructed. This transforms the constraint into an inequality on control inputs, as shown in Eq. (32). The methods for limiting the other three angular velocities are similar. Eq. (33) presents the constraints on the control inputs corresponding to all angular velocity constraints.

$$\underbrace{-[0, 0, 0, -1, 0, 0] \mathbf{g}(\mathbf{x})}_{-L_g B_{\theta}} \mathbf{u} \leq \underbrace{0}_{L_f B_{\theta}} + \underbrace{0.3 - \dot{\theta}_y}_{\alpha(B_{\theta}), \alpha(B_{\theta})=B_{\theta}}, \quad (32)$$

$$\begin{bmatrix} 0, 0, 0, 1, 0, 0 \\ 0, 0, 0, -1, 0, 0 \\ 0, 0, 0, 0, 0, 1 \\ 0, 0, 0, 0, 0, -1 \end{bmatrix} \mathbf{g}(\mathbf{x}) \mathbf{u} \leq \begin{bmatrix} 0.2 - \dot{\theta}_y \\ 0.2 + \dot{\theta}_y \\ 0.2 - \dot{\theta}_r \\ 0.2 + \dot{\theta}_r \end{bmatrix}. \quad (33)$$

The final control input \mathbf{u}^* that ensures system safety can be obtained by combining Eqs. (31)(33) to solve the QP in

TABLE II
PERFORMANCE OF THE DESIGNED CBF FOR DIFFERENT c_1 VALUES.

c_1	0.5	1.0	1.1	1.2	1.3	1.4	1.5	2.0
$N_{u,s}$	22	3	3	2	2	1	0	0
$N_{s,u}$	56	94	96	106	113	118	132	178
Accuracy	99.22%	99.03%	99.01%	98.92%	98.86%	98.81%	98.68%	98.22%

*Notes: $N_{s \rightarrow u}$ represents the number of safe samples identified as unsafe, and $N_{u \rightarrow s}$ represents the number of unsafe samples identified as safe. Accuracy represents the ratio of correctly identified samples.

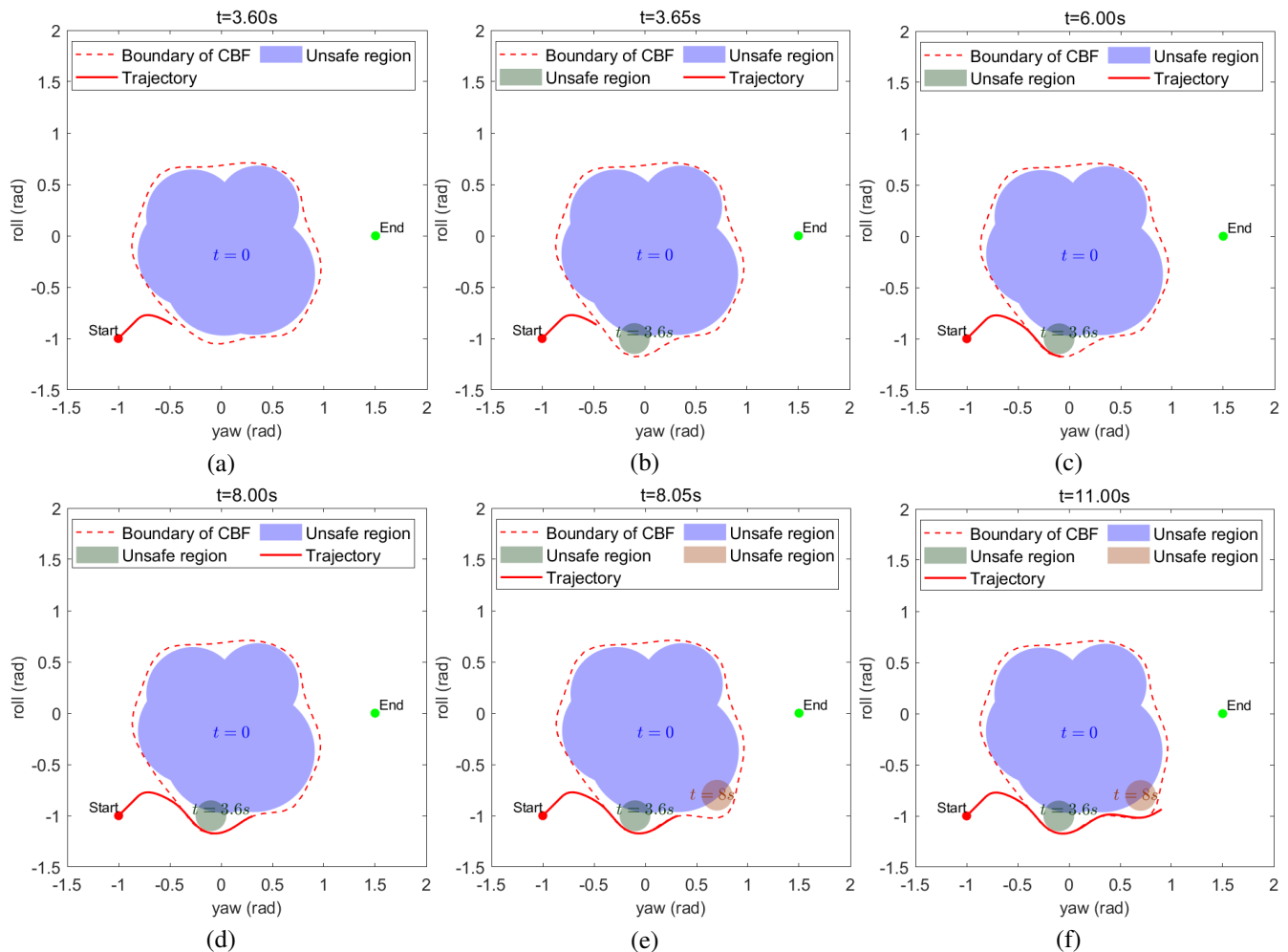


Fig. 7. The trajectories at different times: (a) before the first region change, (b) after the first region change, (c) between the two region changes, (d) before the second region change, (e) after the second region change, (f) after some time following the region change.

Eq. (8). The trajectory of states is illustrated in Fig. 7. It can be observed that each time the unsafe region changes, the boundary of designed CBF is able to quickly update to encompass the whole unsafe region, maintaining safety even when the newly added unsafe area lies along the trajectory at a short distance. Meanwhile, the control inputs and angular velocities, as illustrated in Fig. 6, remain within the defined safety range. By comparison, Fig. 8 shows the trajectory when the CBF is not updated, indicating that the state will enter the unsafe region without updates.

Finally, the training and updating time consumption of the

proposed method are compared with those of the SVM-based CBF and MLP-based CBF, as summarized in Table III. The SVM employs a Gaussian kernel, while the MLP consists of three hidden layers, each containing 10 neurons. The proposed method demonstrates a significant advantage in both training and updating time consumption, making it well-suited to meet real-time control requirements.

V. CONCLUSIONS

In this paper, we have introduced the cost-sensitive incremental RVFL to construct the CBF. By adding a cost-sensitive term to the cost function of the RVFL, the boundary

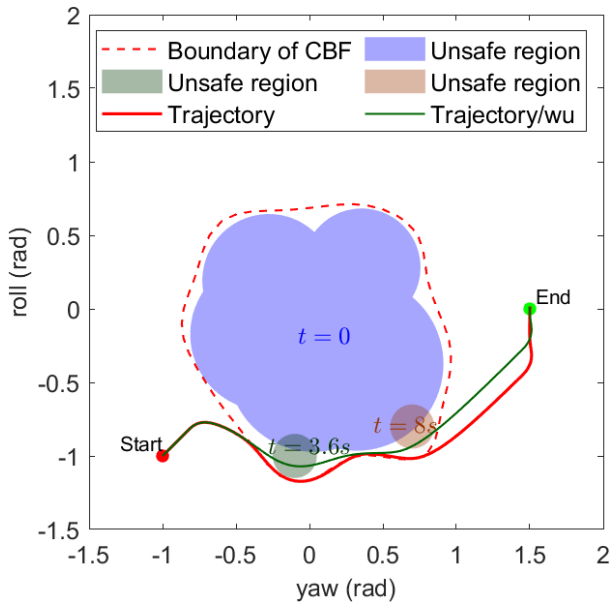


Fig. 8. Trajectories of states. *Trajectory* represents the trajectory of the proposed method, while *Trajectory/wu* represents the trajectory when the CBF is not updated.

TABLE III

THE TIME (S) TAKEN FOR TRAINING AND UPDATING (OVER 5 RUNS)

Period	SVM-CBF [11]	MLP-CBF [13]	Proposed*
Train	0.3207 ± 0.0259	4.0890 ± 0.0260	0.0316 ± 0.0021
First update	0.3135 ± 0.0193	4.1236 ± 0.0401	0.0053 ± 0.0006
Second update	0.3317 ± 0.0207	4.1085 ± 0.0150	0.0051 ± 0.0004

of the designed CBF can effectively enclose the unsafe regions, ensuring the safety of the system. An incremental update theorem for the designed CBF has been proposed, enabling real-time updates when the unsafe region changes. Experiments on a 3-degree-of-freedom attitude control system have validated the effectiveness in safety-critical control and real-time updating. In the future, we will explore the theoretical guarantees of safety provided by explicit gradients and their contribution to the feasibility properties of QP. And the potential of proposed method for enabling drones to autonomously adjust attitude angles to avoid high-speed moving obstacles will be further considered.

REFERENCES

- [1] Z. Liu, S. Hu, and X. He, "Real-time safety assessment of dynamic systems in non-stationary environments: A review of methods and techniques," in *2023 CAA Symposium on Fault Detection, Supervision and Safety for Technical Processes (SAFEPROCESS)*. IEEE, 2023, pp. 1–6.
- [2] H. Xiao, L. Ze-Yi, H. Song-Qiao, L. Chang, and Z. Dong-Hua, "Real-time safety assessment techniques of dynamic systems," *Acta Automatica Sinica*, vol. 51, no. 2, pp. 249–270, 2025.
- [3] F. Blanchini, "Set invariance in control," *Automatica*, vol. 35, no. 11, pp. 1747–1767, 1999.
- [4] A. D. Ames, X. Xu, J. W. Grizzle, and P. Tabuada, "Control barrier function based quadratic programs for safety critical systems," *IEEE*

- Transactions on Automatic Control*, vol. 62, no. 8, pp. 3861–3876, 2016.
- [5] K. P. Tee, S. S. Ge, and E. H. Tay, "Barrier lyapunov functions for the control of output-constrained nonlinear systems," *Automatica*, vol. 45, no. 4, pp. 918–927, 2009.
- [6] S. Prajna and A. Jadbabaie, "Safety verification of hybrid systems using barrier certificates," in *International Workshop on Hybrid Systems: Computation and Control*. Springer, 2004, pp. 477–492.
- [7] M. Rauscher, M. Kimmel, and S. Hirche, "Constrained robot control using control barrier functions," in *2016 IEEE/RSJ International Conference on Intelligent Robots and Systems (IROS)*. IEEE, 2016, pp. 279–285.
- [8] W. Xiao, T.-H. Wang, R. Hasani, M. Chahine, A. Amini, X. Li, and D. Rus, "Barriernet: Differentiable control barrier functions for learning of safe robot control," *IEEE Transactions on Robotics*, vol. 39, no. 3, pp. 2289–2307, 2023.
- [9] J. Breeden and D. Panagou, "Robust control barrier functions under high relative degree and input constraints for satellite trajectories," *Automatica*, vol. 155, p. 111109, 2023.
- [10] K. Zhao and Y. Song, "Decision function-based adaptive control of uncertain systems subject to irregular output constraints," *IEEE Transactions on Automatic Control*, 2024.
- [11] M. Srinivasan, A. Dabholkar, S. Coogan, and P. A. Vela, "Synthesis of control barrier functions using a supervised machine learning approach," in *2020 IEEE/RSJ International Conference on Intelligent Robots and Systems (IROS)*. IEEE, 2020, pp. 7139–7145.
- [12] W. Xiao, C. G. Cassandras, and C. A. Belta, "Learning feasibility constraints for control barrier functions," in *2023 European Control Conference (ECC)*. IEEE, 2023, pp. 1–6.
- [13] A. Robey, H. Hu, L. Lindemann, H. Zhang, D. V. Dimarogonas, S. Tu, and N. Matni, "Learning control barrier functions from expert demonstrations," in *2020 59th IEEE Conference on Decision and Control (CDC)*. IEEE, 2020, pp. 3717–3724.
- [14] S. Chen, Z. Wu, and P. D. Christofides, "Machine-learning-based construction of barrier functions and models for safe model predictive control," *AICHE Journal*, vol. 68, no. 6, p. e17456, 2022.
- [15] Z. Liu and X. He, "Online dynamic hybrid broad learning system for real-time safety assessment of dynamic systems," *IEEE Transactions on Knowledge and Data Engineering*, vol. 36, no. 12, pp. 8928–8938, 2024.
- [16] Z. Liu, X. He, B. Huang, and D. Zhou, "A review on incremental learning-based fault diagnosis of dynamic systems," *Authorea Preprints*, 2024.
- [17] S. Sastry, *Nonlinear systems: analysis, stability, and control*. Springer Science & Business Media, 2013, vol. 10.
- [18] A. D. Ames, S. Coogan, M. Egerstedt, G. Notomista, K. Sreenath, and P. Tabuada, "Control barrier functions: Theory and applications," in *2019 18th European control conference (ECC)*. IEEE, 2019, pp. 3420–3431.
- [19] A. D. Ames, J. W. Grizzle, and P. Tabuada, "Control barrier function based quadratic programs with application to adaptive cruise control," in *53rd IEEE conference on decision and control*. IEEE, 2014, pp. 6271–6278.
- [20] W. Xiao and C. Belta, "High-order control barrier functions," *IEEE Transactions on Automatic Control*, vol. 67, no. 7, pp. 3655–3662, 2021.
- [21] Y.-H. Pao, G.-H. Park, and D. J. Sobajic, "Learning and generalization characteristics of the random vector functional-link net," *Neurocomputing*, vol. 6, no. 2, pp. 163–180, 1994.
- [22] Z. Liu and X. He, "Dynamic submodular-based learning strategy in imbalanced drifting streams for real-time safety assessment in nonstationary environments," *IEEE Transactions on Neural Networks and Learning Systems*, vol. 35, no. 3, pp. 3038–3051, 2023.
- [23] W. W. Hager, "Updating the inverse of a matrix," *SIAM review*, vol. 31, no. 2, pp. 221–239, 1989.
- [24] Quanser, "3 DOF Hover," <https://www.quanser.com/products/3-dof-hover/>, 2025, accessed: 2025-02-26.